In-flight melting mechanism of granulated powders for glass production by argon-oxygen induction thermal plasmas

M. M. Hossain[1], Y. Yao[1], Y. Oyamatsu[1], T. Watanabe[1], F. Funabiki[2], and T. Yano[2]

[1]*Department of Environmental Chemistry and Engineering*
Tokyo Institute of Technology, G1-22, 4259 Nagatsuta, Yokohama 226-8502, Japan
[2]*Department of Chemistry and Materials Science, Tokyo Institute of Technology*
S7-4, 2-12-1 O-okayama, Tokyo 152-8550, Japan

Abstract: To investigate the heat exchange dynamics between plasma and particles during in-flight melting of granulated powders, a plasma-particle interaction model has been developed. This model solves the conservation equations to predict the temperature and flow fields of plasma, under LTE conditions and then calculates the injected particles trajectories and temperature histories, and the particle source terms. It is found that particle injection reduces the plasma temperature around the centerline of the torch and hence decreases the heat transfer to particles at higher powder feed-rate.

Keywords: Heat transfer, particle temperature, soda-lime glass, vitrification degree.

1. Introduction

Induction thermal plasmas (ITP) have extensively been used for the synthesis and surface treatment of fine powders since couple of decades as a clean reactive heat source [1]. ITP technology ensures essentially the in-flight one-step melting, short melting time, and less pollution compared with the traditional technologies that have been using in the glass industries for the vitrification of granulated powders. Our aim is to determine the in-flight melting mechanism of soda-lime glass powders by ITP and to optimize the discharge parameters that affect the quenched powders size and compositions. The thermal treatment of injected particles depends mainly on the plasma-particle heat transfer efficiency, which in turn depends to a large extent on the trajectory and temperature history of the injected particles. Thus, it is the challenge to predict the trajectory and temperature history of the particles injected into the ITP torch. Boulos [2] developed a model and discussed the plasma-particle heat exchange dynamics for argon plasma. Later Proulx *et al* [3] predicted the trajectory and temperature history of metallic particles injected into ITP torch and discussed the particle loading effects for argon plasma. To achieve our goal, based on Ref. [3], a model has been developed for argon-oxygen plasma, including a metal tube inserted into the torch for the injection of carrier gas and granulated glass powders. This model can be used to demonstrate the particle loading effects and to optimize the parameters that govern the particles trajectory, temperature, and plasma-particle energy exchange.

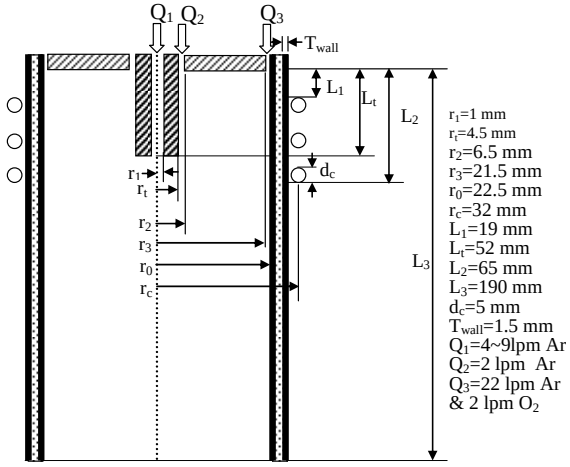

Fig.1 Schematic geometry and dimensions of ITP torch

2. Modeling

2.1 Plasma model

The schematic geometry and dimensions of ITP torch is presented in Fig.1. The model solves the conservation equations and vector potential form of Maxwell's equations simultaneously under LTE conditions, including a metal tube inserted into the torch. It is assumed that plasma flow is 2-dimensioanl, axi-symmetric, laminar, steady, optically thin, and electromagnetic fields are 2-dimensional. Adding the source terms to the conservation equations, the plasma-particle interaction and loading effects of powder injected into the torch, has been taken into account. In this model, the conservation equations are as follows:

Mass conservation:

$$\nabla \cdot \rho \mathbf{u} = S_p^C \qquad (1)$$

Momentum conservation:

$$\rho \mathbf{u} \cdot \nabla \mathbf{u} = -\nabla p + \nabla \cdot \mu \nabla \mathbf{u} + \mathbf{J} \times \mathbf{B} + S_p^M \qquad (2)$$

Energy conservation:

$$\rho \mathbf{u}\cdot\nabla h = \nabla\cdot\left(\frac{\kappa}{C_p}\nabla h\right) + \mathbf{J}\cdot\mathbf{E} - Q_r - S_p^E \qquad (3)$$

Species conservation:

$$\rho \mathbf{u}\cdot\nabla y = \nabla\cdot\left(\rho D_m \nabla y\right) + S_p^C \qquad (4)$$

Vector potential form of Maxwell field equation [4]:

$$\nabla^2 \mathrm{A_c} = i\mu_0\sigma\omega\mathrm{A_c} \qquad (5)$$

Where, ∇: vector operator, **u**: velocity vector, ρ: mass density, μ: viscosity, σ: electrical conductivity, κ: thermal conductivity, h: enthalpy, p: pressure, C_p: specific heat at constant pressure, D_m: multicomponent diffusion coefficient, y: mass fraction, **J**: current density vector, **E**: electric field vector, **B**: magnetic field vector, Q_r: volumetric radiation loss, A_c: complex amplitude of vector potential, μ_0: permeability of free space, ω: $2\pi f$ (f: frequency), i: complex vector ($\sqrt{-1}$). The particle source terms S_p^C, S_p^M and S_p^E are the contributions of particles to the mass and species, momentum and energy conservation equations respectively.

The boundary conditions, thermodynamic and transport properties of argon and oxygen gases and calculation procedure are the same as those described in our previous work [5].

2.2 Particle model

The following assumptions are made in the analysis of plasma-particle interactions; the particle motion is two-dimensional, only the viscous drag force and gravity affect the motion of an injected particle, the temperature gradient inside the particle is neglected, and the particle charging effect caused by the impacts of electrons or positive ions is negligible. The electromagnetic drag forces caused by the particle charging of the injected powder are negligible compared with those by neutrals and charged particles due to negligible electrical conductivity of soda-lime powders. Thus, the momentum equations for a single spherical particle injected vertically downwards into the plasma torch can be expressed as:

$$\frac{du_p}{dt} = -\frac{3}{4}C_D(u_p - u)U_R\left(\frac{\rho}{\rho_p d_p}\right) + g \qquad (6)$$

$$\frac{dv_p}{dt} = -\frac{3}{4}C_D(v_p - v)U_R\left(\frac{\rho}{\rho_p d_p}\right) \qquad (7)$$

$$U_R = \sqrt{(u_p - u)^2 + (v_p - v)^2} \qquad (8)$$

The particle temperature, liquid fraction and diameter are predicted according to the following energy balances:

$$Q = \pi d_p^2 h_c\left(T - T_p\right) - \pi d_p^2 \sigma_s \varepsilon\left(T_p^4 - T_a^4\right) \qquad (9)$$

$$\frac{dT_p}{dt} = \frac{6Q}{\pi\rho_p {d_p}^3 C_{pp}}, \qquad T_p < T_b \qquad (10)$$

$$\frac{dx}{dt} = \frac{6Q}{\pi\rho_p {d_p}^3 H_m}, \quad 1000 \le T_\mathrm{p} \le 1600 \qquad (11)$$

$$\frac{dd_p}{dt} = -\frac{2Q}{\pi\rho_p {d_p}^2 H_v}, \quad 1000 \le T_\mathrm{p} \le 1600, \; T_p \ge T_b \qquad (12)$$

where u_p: axial velocity component of particle, v_p: radial velocity component of particle, g: acceleration of gravity, ρ_p: particle mass density, d_p: particle diameter, Q: the net heat exchange between the particles and its surroundings, T_p, T_m and T_b: particle temperature, melting point temperature and boiling point temperature, respectively, T: plasma temperature, T_a: ambient temperature, ε: particle surface emissivity; σ_s: Stefan-Boltzmann constant, C_{pp}: particle specific heat, H_m and H_v: latent heat of particle melting and vaporization respectively, and x: the liquid mass fraction of the particle.

Drag coefficient C_{Df} is calculated using equation (13) and the property variation at the particle surface layer and the non-continuum effects are taken into account by equation (14) and (15) respectively [6].

$$C_{D\mathrm{f}} = \begin{cases} \dfrac{24}{R_e} & R_e \le 0.2 \\ \dfrac{24}{R_e}\left(1 + \dfrac{3}{16}R_e\right) & 0.2 < R_e \le 2.0 \\ \dfrac{24}{R_e}\left(1 + 0.11{R_e}^{0.81}\right) & 2.0 < R_e \le 21.0 \\ \dfrac{24}{R_e}\left(1 + 0.189{R_e}^{0.62}\right) & 21.0 < R_e \le 200 \end{cases} \qquad (13)$$

$$f_1 = \left(\frac{\rho_\infty \mu_\infty}{\rho_\mathrm{s}\mu_\mathrm{s}}\right)^{-0.45} \qquad (14)$$

$$f_2 = \left\{1 + \left(\frac{2-\alpha}{\alpha}\right)\left(\frac{\gamma}{1+\gamma}\right)\frac{4}{Pr_s}Kn\right\}^{-0.45}, \quad 10^{-2}<Kn<0.1 \quad (15)$$

$$C_D = C_{Df} f_1 f_2 \quad (16)$$

To take into account the steep temperature gradient between plasma and particle surface, the Nusselt correlation can be expressed by equation (17) [7]. The non-continuum effect is taken into account by equation (18) [6].

$$Nu_f = (2.0 + 0.6 R_{ef}^{1/2} Pr_f^{1/3})\left(\frac{\rho_\infty \mu_\infty}{\rho_s \mu_s}\right)^{0.6}\left(\frac{C_{p\infty}}{C_{ps}}\right)^{0.38} \quad (17)$$

$$f_3 = \left\{1 + \left(\frac{2-\alpha}{\alpha}\right)\left(\frac{\gamma}{1+\gamma}\right)\frac{4}{Pr_s}Kn\right\}^{-1}, \quad 10^{-3}<Kn<0.1 \quad (18)$$

The convective heat transfer coefficient is predicted as follows:

$$h_{cf} = \frac{\kappa_f}{d_p} Nu_f f_3 \quad (19)$$

In the above expressions, subscript f, ∞ and s refer to properties corresponding to the film temperature (arithmetic mean of plasma and particle temperatures), plasma temperature and particle temperature respectively, C_{pp}: particle specific heat, ρ_p: particle mass density, h_c: heat transfer coefficient, *Nu*: Nusselt number, *Pr*: Prandtl number, *Re*: Reynold number, $\propto$: thermal accommodation coefficient, γ: specific heat ratio and *Kn*: Knudsen number. The physical properties of soda-lime glass powders are: mass density 2300 kg/m^3, specific heat 800 J/kg-K, surface emissivity 80%, fusion and boiling temperature 1000~1600 K and 2500 K respectively, heat of fusion, and vaporization 3.69×10^5 J/kg and 1.248×10^7 J/kg, respectively.

2.3 Particle source terms

For the sake of computation, the particle concentration in the inlet is assumed to be uniform and to be separated into five injection points, which are at radial positions of 0.3, 0.45, 0.6, 0.75 and 0.9 mm. In the present computation, the particle size distribution is the same as that of experiment. There are seven diameters of particles and the average powder diameter is 58 μm with the maximum deviation of 67%. As a result, that gives rise to 35 different possible particle trajectories. The injection velocity of the particles is assumed to be equal to the initial velocity of carrier gas. To take into account the particle loading effects the particle source terms for the mass, momentum, energy and species conservation equations have been calculated in the same fashion as described in Ref. [3] using the PSI-Cell (Particle-Source-In Cell) approach [8] where the particles are regarded as sources of mass, momentum and energy.

After having the conversed plasma temperature and velocity with zero powder feed-rate, particle trajectories and temperature histories as well as the particle source terms are calculated with certain feed-rate. Incorporating the particle source terms, back calculations of plasma fields and with the new plasma fields again the particle temperature and trajectories are calculated. This process is repeated until convergence.

3. Simulated results

The experimental discharge is sustained at 20 kW plug power, 4 MHz induction frequency, and 0.1 MPa pressure. The overall efficiency of the reactor is assumed to be 50%, thus, plasma power is set to 10 kW. The simulated plasma temperature distributions are shown in Fig.2. The carrier gas flow-rate is 6 lpm argon. This figure clearly depicts that higher powder feed-rate cools the plasma around the torch centerline and has insignificant effects away from the centerline. Fig.3 reveals that higher carrier gas flow-rate and powder feed-rate decrease the particle temperature which indicates less heat transfer to particles. Because, higher carrier gas flow-rate causes lower plasma temperature and renders less residence time. Higher powder feed-rate requires much heat energy to melt and vaporize the particles; thus, it causes serious local cooling of plasma around the centerline. And lower plasma temperature causes less heat transfer to particles; as a result higher feed-rate decreases the particle temperature.

4. Experimental

Experiments have been carried out for the same discharge conditions as presented in Fig.1. The powder feed rate is 5-20 g/min and the mean diameter of the feed powder is 58 μm. The composition of feed powder is Na_2O: 16, CaO: 10 and SiO_2: 74 wt%.

5. Experimental results and discussion

Fig.4 shows the XRD and ICP-ES spectrum analysis results for a carrier gas flow-rate of 6 lpm. It is found that the content of Na_2O in the quenched powder increases whereas the vitrification degree decreases with the increase of feed-rate. Evaporation of Na_2O depends on particle temperature; the lower the particle temperature, the smaller the evaporation rate. These results indicate that higher feed-rate causes smaller heat transfer rate, thus less

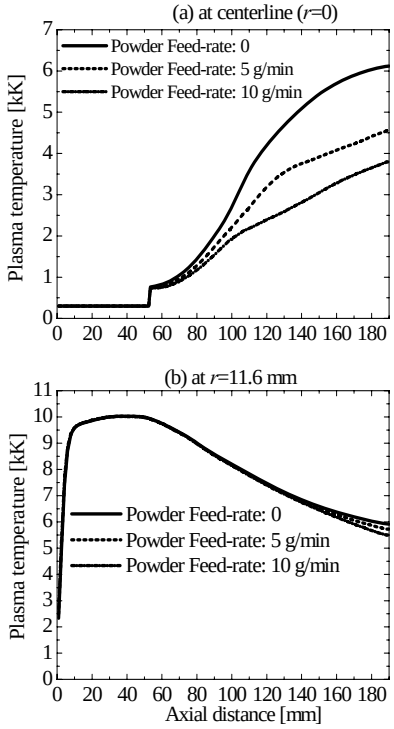

Fig.2 Powder loading effects on the plasma temperature at r=0 (a) and r=11.6 mm (b).

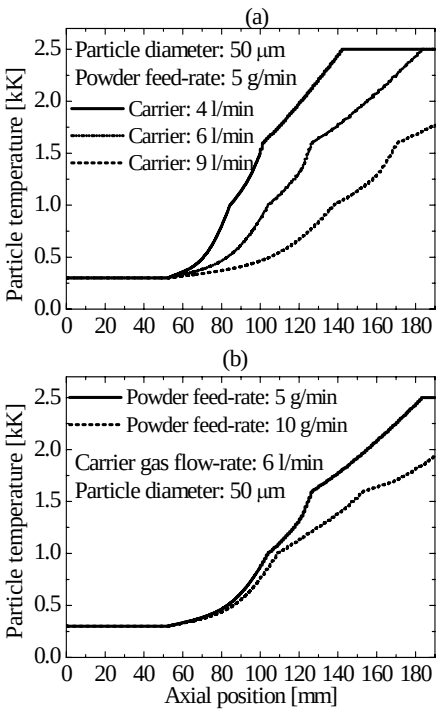

Fig.3 Effects of carrier gas (a), and powder feed-rate (b) on particle temperature history

evaporization of Na_2O. Also the lower vitrification degree at higher feed-rate reflects the smaller heat transfer rate. From the simulated results it is also evident that at higher carrier gas flow-rate and powder feed–rate, particle temperature decreases, that clearly point the decreased heat transfer rate to particles at higher feed-rate. Thus, the simulated results are inline with the experimental findings.

6. Conclusions

The developed model can be used to optimize the carrier gas flow-rate, particle size, and powder feed-rate to achieve the maximum treatment efficiency during thermal treatment of granulated powders by mixed-gas induction thermal plasmas. Numerically, it is found that the heat transfer to particles decreases at increased carrier gas flow-rate and powder feed-rate, and these results well agree with those of experiment. Thus, it can be concluded that, efficient thermal treatment of particles depends not only on the physical properties of the particles, but also on the plasma discharge conditions and particle parameters. Therefore, for a particular type of powder (certain physical properties) both carrier gas flow-rate and powder feed-rate mainly determine the treatment quality.

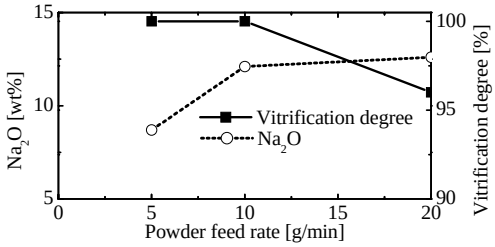

Fig.4 Effects of powder feed-rate on vitrification degree and Na_2O content in quenched powder

References

[1] T. Watanabe and K. Fujiwara, *Chem. Eng. Comm*., **191**, 1343 (2004).
[2] M. I Boulos, *IEEE Trans. on Plasma Sci*, **PS-6**, 93 (1978).
[3] P. Proulx, J. Mostaghimi and M. I Boulos, *Int. J. Heat Mass Transfer*, **28**, 1327 (1985).
[4] J. Mostaghimi, K. C Paul and T. Sakuta, *J. Appl. Phys.*, **83**, 1898 (1998).
[5] M. M. Hossain, Y. Yao, Y. Oyamatsu, T. Watanabe, F. Funabiki and T. Yano, *WSEAS Trans. Heat and Mass Transfer*, **1**, 625 (2006).
[6] X. Chen and E. Pfender, *Plasma Chem. Plasma Process*. **3**, 97 (1983).
[7] Y. C. Lee, Y. P. Chyou, and E. Pfender, *Plasma Chem. Plasma Process.* **5**, 391 (1985).
[8] C. T Crowe, M. P Sharma and D. E Stock, *J. Fluid Eng.*, **99**, 325 (1977).